# Improved Correction for Hot Pixels in Digital Imagers

Glenn H. Chapman, Rohit Thomas, Rahul Thomas

School of Engineering Science
Simon Fraser University
*Burnaby, B.C., Canada, V5A 1S6*
glennc@ensc.sfu.ca, rpt4@sfu.ca, rmt3@sfu.ca

Israel Koren, Zahava Koren

Dept. of Electrical and Computer Engineering
University of Massachusetts
Amherst, MA, 01003
*koren,zkoren@ecs.umass.edu*

*Abstract*— **From extensive study of digital imager defects, we found that "Hot Pixels" are the main digital camera defects, and that they increase at a nearly constant temporal rate over the camera's lifetime. Previously we characterized the hot pixels by a linear function of the exposure time in response to a dark frame setting. Using a camera with 55 known hot pixels, we compared our hot pixel correction algorithm to a conventional 4-nearest neighbor interpolation techniques. We developed a new "moving camera" method to exactly obtain both the actual hot pixel contribution and the true undamaged pixel value at a defect. Using these calibrated results we find that the correction method should be based on the hot pixel severity, the illumination intensity at the pixel, camera parameters such as ISO and exposure time, and on the neighboring pixels' variability.**

*Keywords- imager defect correction, hot pixel, active pixel sensor APS, CCD, ISO*

## I. INTRODUCTION

The area of Digital Imaging and its associated technology has become a central theme in today's world of photography. Digital imagers have spread into everyday devices ranging from consumer products such as cell phones to cars via embedded sensors. Their role in medical, industrial, and scientific applications is becoming more and more vital in many engineering solutions. The inherent result is a drive to enhance these sensors via a decrease in pixel size and an increase in the sensitivity of the imager. As with other microelectronic devices, digital imagers develop defects over time, and the nature of the sensor makes it more sensitive to defects that most likely would not affect other devices. However, in contrast to other devices, in-field defects in digital imagers begin to manifest themselves soon after fabrication. These defects are permanent and continuously increase in number over the sensor's lifetime, eventually degrading image quality. This is a serious problem for various applications where image quality/pixel sensitivity is important.

Our research for the past several years has focused on the investigation of in-field imager defects, specifically their development, characterization, and rate [1-6]. Our recent studies resulted in an empirical formula, which projects that as the pixel size shrinks, and the sensitivity increases, defect numbers will grow via a power law of inverse of the pixel size to the 3.3. This formula predicts that as pixel sizes drop below two microns, and sensitivities trend towards those for low light night pictures, defect rates can grow to hundreds or even thousands per year in typical cameras. This model of the defect rate is a function of the ISO, pixel size and sensor area. Additionally, we have shown [1-3] that the in-field defect causal mechanism is most likely cosmic ray damage, which cannot be protected against by methods such as shielding. Given that the development of these defects in the sensor is continuous, it is important to study their characteristics and behavior and suggest a method of correcting them

With this model of hot pixel behavior, the conventional correction method based on simple averaging of the faulty pixel's neighbors may not yield ideal results due to the large number of corrections, and as one or more of the neighbors could also be faulty. . We suggest a novel algorithm to correct faulty pixels based on their hot pixel parameters. We then experimentally compare the correction of our algorithm to that of conventional interpolation methods. . Even with this ability to correct hot pixel defects with greater accuracy by knowing the pixel defect parameters, we are still left with some amount of error in our correction. To assess the effectiveness of any correction algorithms, we need to compare the corrected value to the true pixel value. In the past, we used complicated methods to approximate the true value of a defective pixel. In this paper, we use a simpler but very accurate method to extract the true value of the defective pixel, by moving the camera. This procedure can, unfortunately, be performed only in lab conditions, but we found it useful to assess the accuracy of our different correction algorithms.

This paper is organized as follows: Section II presents the classical model of imager *hot pixels*. Section III describes the growth rate of the hot pixels. Section IV presents our novel defect correction algorithm. Section V describes the numerical experiments we performed to validate the effectiveness of our algorithm, and Section VI discusses possible correction limitations. Finally, Section VII concludes the paper.

## II. HOT PIXELS

Over the past 10 years [5,6], we have been studying the characteristics of imager defects by manually calibrating many commercial cameras, including 24 Digital Single Lens Reflex (DSLRs), by exposing them to dark fields (i.e., no illumination). This helps us to identify stuck-high and partially stuck defects. Up till now, we have not identified any stuck pixel types in our experiments. The prominent defect types are hot pixels. The standard hot pixel has a dark response that has an illumination-independent component that increases linearly

with exposure time, and can, therefore, be identified by capturing a series of dark field images at increasing exposure times. Figure 1 displays the dark response of a hot pixel, showing the normalized pixel illumination vs. the exposure time where illumination level 0 represents no illumination and level 1 represents saturation. Three different pixel responses are shown in Figure 1. Firstly a good pixel is displayed as curve (a). Since there is no illumination, we expect the pixel output to be constantly zero for all exposures. The other two curves depict the 2 different types of hot pixels [5]. Curve (b) is a standard hot pixel which has an illumination-independent component that increases linearly with exposure time. The third response shown as curve (c) is a partially stuck hot pixel which has an additional offset that manifests at no exposure.
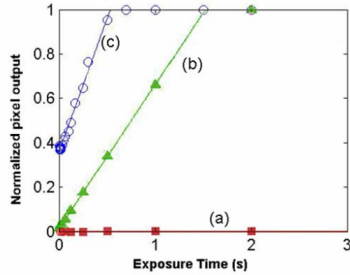


Figure 1: Comparing the dark response of imager pixels (a) good pixel, (b) standard hot pixel, (c) hot pixel with offset.

The imager is generally referred to as a digital system, but the main pixel sensor is an analog device. The classic assumed response of good and hot pixels to illumination can be modeled using Equation (1), where $I_{pix}$ is the response, $R_{photo}$ measures the incident illumination rate, $R_{dark}$ is the dark current rate, $T_e$ measures of the exposure time, b is the dark offset, and m is the amplification from the ISO setting.

$$I_{pix}(R_{photo},R_{dark},T_e,b)=m*(R_{photo}\ T_{exp}+R_{dark}\ T_e+b) \qquad (1)$$

For a good pixel, both $R_{dark}$ and b are zero, resulting in the output response being a direct measure of the incident illumination. However, for the case of hot pixels, these two terms create a signal that is added onto the incident illumination, and therefore the pixel output appears to be brighter. To estimate the dark response of a pixel, $I_{offset}$, can be found by setting $R_{photo}$ to zero which yields

$$I_{offset}(R_{dark},T_e,b)=m*(R_{dark}T_e+b) \qquad (2)$$

The dark response equation in Equation (2), sometimes called the combined dark offset, is linear. Thus, the parameters $R_{dark}$ and b can be extracted by fitting the pixel response in a dark frame vs. exposure time, as seen in Figure 1. For standard hot pixels, b is zero. These hot pixels are most visible in longer exposures as they do not have an initial offset. In the partially stuck hot pixel case, the magnitude of b affects the response. This defect will appear in all images. Obtaining this data for each camera involves typically 5 to 20 calibration images per test at a wide range of exposure times and ISO's, and their analysis with specialized software [2-4].

We have identified hot pixels from 24 DSLR cameras including both APS and CCD sensors, with the age of these cameras varying between 1 and 10 years [9]. Our results showed a cumulative total of 243 hot pixels of which 44% were of the partially stuck type, after performing the dark-frame calibration at ISO 400. Partially stuck hot pixels have a greater impact on the image quality since the offset in such hot pixels causes it to appear at any exposure level. The ISO setting in an imager controls the amplification or sensitivity of the pixel output. Higher ISO settings enable objects to be captured under low light conditions or with very short exposures. Therefore, this removes the need for flash or a long exposure time when doing natural light photography. The amplification level scales proportionally with the ISO setting, but the usable ISO range is limited by the noise level of the sensor. Twelve years ago, most commercial DSLRs had a usable ISO range of 100 – 1600. As sensor technology improved and better noise reduction algorithms were developed, noise levels have been reduced and the usable ISO range has increased considerably, with recent DSLRs having an ISO range of 50 to 12,300 and high-end cameras having a range from 25,600 to 409,600 ISO.

The high number of hot pixels with offsets suggests that the development of stuck high pixels in the field may actually be due to the presence of hot pixels with very high offsets. This is consistent with our experience of not having detected a true stuck pixel in any of our cameras, while explaining the cameras developing stuck pixels discussed in camera forums.

## III. DEFECT GROWTH RATE

Over the past few years we have studied the defect growth rates of hot pixels. Our research has shown that hot pixel defects occur randomly over the imager [1-6], indicating a source that is also random in nature, most likely cosmic rays. These results have also been observed by other authors, and they have shown that neutrons seem to create the same hot pixel defect types [7,8]. We recently developed, in [9], an empirical formula to relate the defect density D (defects per year per $mm^2$ of sensor area) to the pixel size S (in microns) and sensor gain (ISO) via the following equations:

For APS pixels: $D=10^{-1.13}\ S^{-3.05}ISO^{0.505}$      (3)

For CCD sensors $D=10^{-1.849}\ S^{-2.25}ISO^{0.687}$      (4)

These equations show us that the defect rate increases drastically when the pixel size falls below 2 microns, and is projected to reach 12.5 defects/year/$mm^2$ at ISO 25,600 (which is already available on some high-end cameras). Given that the current trend is to reduce the size of pixels, our experimental results project that the number of these defects will increase to high levels, which makes the correction of these defects vital.

## IV. ALGORITHM FOR DEFECT CORRECTION

Digital images are typically modeled as an array of U × V pixels, where $x_{ij}$ denotes the incident illumination at a location (i,j). Each $x_{ij}$ of the digital image is a separate pixel with a value pertaining to certain color. The Bayer Color Filter Array (CFA) [3] is predominantly a repeating pixel color

pattern as shown in Figure 2. This enables each channel, whether red, blue or green to be treated independently. For the purpose of this analysis we will define a repeated CFA pattern as a single CFA pixel. However at image extraction, each individual color is treated as a single pixel.



Figure 2: Bayer Color Filter Array with *k* numbering

The incident illumination of color $k$ ($k$=1,2,3,4 – see Figure 2) can be denoted as $x_{ij}^{(k)}$. We have normalized this value such that $0 \leq x_{ij}^{(k)} \leq 1$.

Extending our previous work[10], we denote by $y_{ij}^{(k)}$ the (standardized) sensor reading of color $k$ in location (*i,j*) (*i*=1,…,U ; *j*=1,…,V ; *k*=1,2,3,4). In the case where there are no defects present, $y_{ij}^{(k)} = x_{ij}^{(k)}$ *for all k=1,…,4.*

Given that the hot pixel defect is small, at most one of the color components per CFA pixel will be hot, and for this $k$

$$y_{ij}^{(k)} = x_{ij}^{(k)} + aT + b \qquad (5)$$

where $aT+b$ is the offset from the hot pixel defect contribution.

The discussion going forward has the indices *i,j,k* removed, but rather numbers the hot (color) pixels *m*=1,…,M (where M is the number of hot pixels). The term $x_m$ denotes the illumination and similarly, $y_m$ denotes the sensor reading of hot (color) pixel *m*. The defective pixel in the center with the surrounding neighbor pixels is shown in Figure 3. Any of the R,G,G,B in the center can be hot.

Our correction algorithm makes use of the following notations

$A_m^{(4)}$ = Conventional corrected value of hot pixel *m* based on 4 neighbors = Average of 4 nearest neighbors

As an example, if the color Red at *i,j* is faulty, then this correction averages the values of R (or *k*=1) for $x_{i-1,j}$ , $x_{i+1,j}$ ,$x_{i,j+1}$, $x_{i,j-1}$
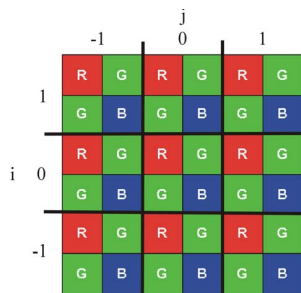


Figure 3: Pixel color array showing surrounding pixels with relative *i,j*

$A_m^{(8)}$ = Conventional corrected value of hot pixel *m* based on 8 neighbors = Average of 8 nearest neighbors

Again, for the color Red (*k*=1) example this averages the red pixels with $x_{i-1,j-1}$ , $x_{i,j-1}$ ,$x_{i+1,j-1}$ , $x_{i-1,j}$ , $x_{i+1,j}$ , $x_{i-1,j+1}$ , $x_{i,j+1}$ ,$x_{i+1,j+1}$

Next, we represent a partially-corrected value based on *dark response* parameters as $D_m$. Recall that obtaining the dark response parameters of a pixel is relatively easy to obtain.

$$D_m = y_m - (aT + b) \qquad (6)$$

It is important to note that the 4 and 8 point interpolation methods are only effective when the 9 pixels of Figure 3 have a illumination that changes slowly for the given color (i.e. a uniform area). This is effectively a tilted plain of that color. These methods fail in a typical busy scene where an edge or sudden change occurs anywhere in that 9-pixel set. This constitutes quite a large area of the camera image, so such changes often occur. Thus, correcting these images using hot pixel parameters may produce better image correction. However, our corrected value $D_m$ (Equation 6) still may not be enough to accurately correct these defects as it is purely based upon curve fitting and darkfield measurements. We therefore suggest the following correction algorithm which uses a weighted combination, denoted by $C_m$ , of $A_m$ and $D_m$ .

In our algorithm, we differentiate between uniform areas on the image and rapidly changing areas by comparing the two averages $A_m^{(4)}$ and $A_m^{(8)}$. If these values differ by less than a threshold ε, the area is considered uniform, otherwise it is considered busy. We use the weights $\alpha$ ,$(1 - \alpha)$ or $\beta$ ,$(1 - \beta)$ depending on whether the neighborhood is uniform or busy, respectively.

**Weighted_Correction_Algorithm:**
*For a hot-pixel value $y_m$*
    *Select $\varepsilon \geq 0$,  $0 \leq \alpha \leq 1$,  $0 \leq \beta \leq 1$*

*If  $y_m \geq 0.99$ (indicating saturation)*
    *replace $y_m$  by  $C_m = A_m^{(4)}$*

*Otherwise (no saturation)*

*If  abs( $A_m^{(4)}$ - $A_m^{(8)}$ ) $\leq \varepsilon$ (indicating a slowly changing area)*
    *replace $y_m$  by  $C_m = \alpha A_m^{(4)} + (1 - \alpha) D_m$* (7)

*Otherwise (indicating sudden changes)*
    *replace $y_m$  by  $C_m = \beta A_m^{(4)} + (1 - \beta) D_m$*

The algorithm parameters ε, α, and β need to be selected empirically.

We next present a new experimental method for measuring the accuracy of the different correction algorithms, based on obtaining the true value of the hot pixel by slightly moving the camera. Clearly this can only be performed under lab conditions.

V. EXPERIMENTAL MEASUREMENTS

To test our algorithm we needed to take an image of a busy scene, similar to typical images taken by photographers. A nearly uniform image (say a uniform gray wall) is not a typical picture and it would not test our algorithm since the

interpolation would always give nearly perfect results. For this test we also require a camera that contains a large number of hot pixels with varying strengths at a single ISO.

In our experiment, we used two of our oldest DSLRs which we have been testing for the last 6 years. One camera is approximately 10 years old, while the other is approximately 6 years old. Both cameras gave us similar results. However we will be only describing the measurements obtained using the newer camera (6 years) as it has 52 hot pixels of varying strengths at the ISO 800 level.

As a test image, we took a picture of a wall of books, so that the scene changes in many places, but all objects are at about the same distance from the camera (Figure 4). This image has areas that are slowly changing, good for the interpolation methods, and other areas that are rapidly changing (edges), where the correction $D_m$ is expected to perform better.

It is important to note that the exposure for the scene was selected so that no picture areas were saturated (i.e., the pixel is at the maximum value where it no longer responds to changes in illumination or to the effect of the hot pixel).



Figure 4: Test image for pixel correction

In our earlier attempts, the problem in experimentally testing our algorithm was that we needed to compare the corrected value to the real value for the defective pixel at the exact location. In previous papers [10], we found that this is clearly not easy to obtain. Our previous method required us to take the same image with a short exposure, keeping each pixel's collected light $RT$ constant in order to reduce the hot pixel effect (Equation (2)). Additionally, we had to perform curve fitting of the hot pixel response for various exposures under the same amount of illumination using a uniform illuminated image. This curve fitting would allow us to subtract the hot pixel effect on the short exposure image of Figure 4 and thus give us the real value at the exact location of the defective pixel. This method worked but there was no reliable way to quantify the error in obtaining the real value; it didn't give us a lot of confidence in the obtained real value. Now we have developed a more reliable and more accurate method to test our algorithm in the lab.

To obtain the real value for the defective pixel, we needed to move the camera to the left (or right) such that the previous image location covered by the defective pixel is now visible. Using a piezoelectric micro-positioner (Figure 5), the camera was moved 128 µm, which is 2 times the pixel width due to the camera lens and the CFA (Figure 3). After the image was translated this distance, the original location where the defective pixel resided is now relocated to a non-defective pixel of the same corresponding CFA color channel (see Figure 6). This enables us to extract the real value for the

defective pixel by looking 2 pixels to the right using the moved image, since the image moved two times the pixel width to the left. It is important to note that this method is not needed in order to do the correction, but rather it helps us measure the error due to each of our correction algorithms.

The added benefit of using this method is that we essentially acquire two sets of images containing hot pixels in which we can obtain the real value for each defective pixel and perform our correction algorithm. The second set is obtained when we use the moved image as the initial position and use the initial image before translation as the "moved" image for the second set.
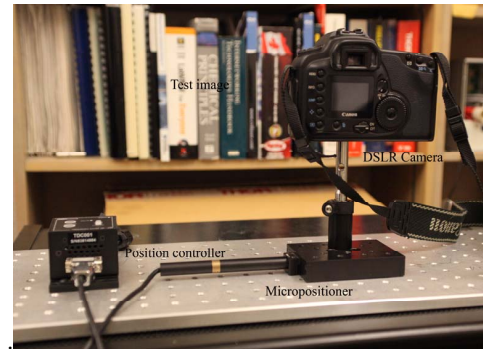


Figure 5: Micropositioner for camera motion
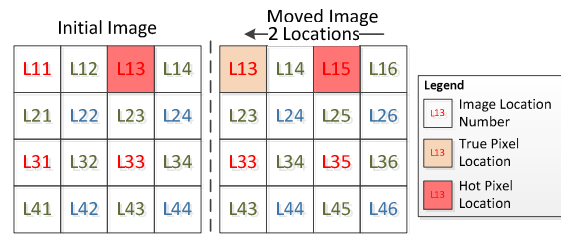


Figure 6: Depiction of Image Movement Method

To quantify the error in this method of extracting the real value, we perform the same extraction method using image locations that do not have defective pixels, comparing the values before and after the translation of the image. By gathering this data for more than 50 pixels, we found an average error of 6.1% of pixel value with a standard deviation of 6.2%. The shot-to-shot experiment repeatability distribution is shown in Figure 7 for the 1/30th exposure (the distribution is very similar for 1/125th exposure). 80% of the errors are <0.004 which is actually below the imager noise floor. Thus the error in this method is almost negligible. The noise floor in our sensor is specified as 0.008 by the manufacturer [11], which lines up with our findings.

From our experiments we see that the hot pixel contribution is initially made up mostly of the dark hot response offset. In Figures 8-9 we can see the distribution of the actual hot pixel contribution and the distribution of the dark hot pixel contribution for 1/30th and 1/125th exposures. It is important to note that even though RT is 0.5 for 1/30th exposure compared to 1/125th exposure, the R for 1/125th exposure is 8x the R for 1/30th exposure due to how we performed the experiments. For this cause we use the dark pixel response value in our correction algorithm.
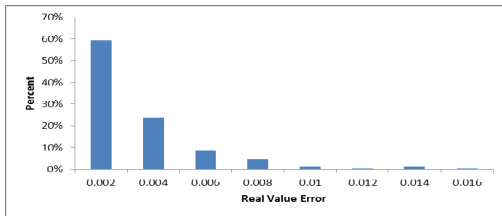
Figure 7: Shot-to-Shot experiment repeatability for 1/30th exposure
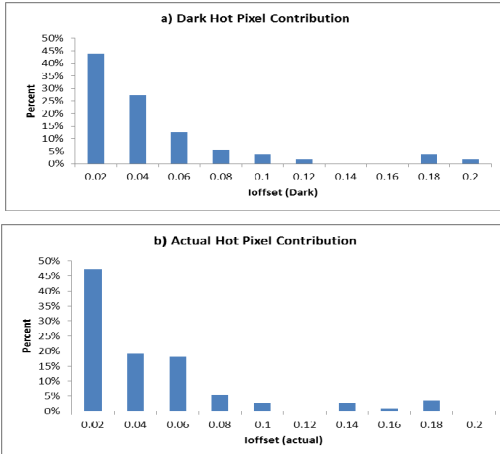

Figure 8: Hot pixel contribution for 1/30$^{th}$ sec exposure (a) calculated from dark hot parameters (b) actual measured hot pixel contribution

However these results show an unexpected problem. In 1/30$^{th}$ exposures (Figure 8) the dark hot pixel parameters give a good estimate of the error created by the defect. However in the 8x brighter 125$^{th}$ scene (Figure 9) the dark parameters (top histogram) show a much smaller defect contribution than the actual defect values.
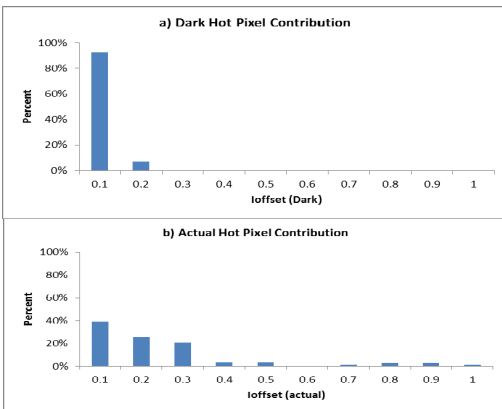

Figure 9: Hot pixel contribution for 1/125$^{th}$ sec exposure (a) calculated from dark hot parameters (b) actual measured hot pixel contribution

After many experiments we came to the conclusion that the presence of sufficient light amplified the hot pixel parameters. This effect is not discussed anywhere in the literature that we could find and becomes an important modification we made in our correction algorithm.

## VI. ANAYSIS OF DEFECT CORRECTION ALGORITHMS

The movement setup gives us a reliable and accurate method to obtain the real pixel value. Using this we can perform the 3 correction methods: interpolation ($A_m^{(4)}$), dark

($D_m$), and weighted ($C_m$)) then compare their results to the real value. We performed the experiment again using a more complex image shown in Figure 10, and took the pictures over various exposure times (1/125$^{th}$ sec to 1/60$^{th}$ sec) at a fixed ISO (800). The reason why we used this image is due to the fact that we were concerned that Figure 4 had too few edges and would inherently favor interpolation. Furthermore, the light intensity ($R$) in Figure 10 test ranges from 0.0226 to 56.24 depending on the exposure times


Figure 10: Higher complexity test image

This image gave us then actual hot pixel contribution distribution ($I_{offset}$) (Figure 11), where the contribution values are well above the noise floor (<= 0.005). By examining this figure we see that even the first bin is well above the noise floor which makes this analysis statistically significant.
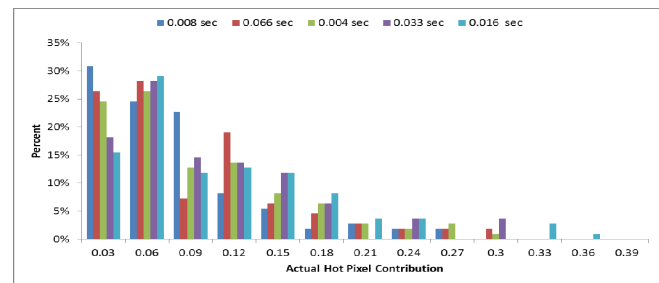

Figure 11: Distribution of Actual Hot Pixel Contribution

Performing the interpolation correction method on the defective pixels to calculate $A_m^{(4)}$, we obtain resulting the error distribution of $A_m^{(4)}$ as shown in Figure 12. This error was obtained by the absolute value of $A_m^{(4)}$ subtracted from the real pixel value. Examining the figure shows us that the interpolation correction method was effective since most of the pixels are in the first 4 bins. The first 4 bins represent the error below the noise floor (0.008).
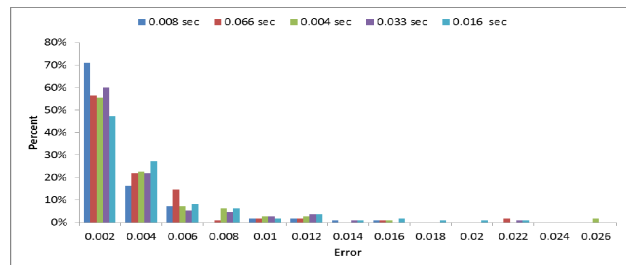

Figure 12: Error distribution of $A_m^{(4)}$

Performing the dark correction method on the defective pixels to calculate $D_m$, we obtain the error distribution of $D_m$ as shown in Figure 13. Again, this error distribution was obtained by the absolute value of $D_m$ subtracted from the real pixel

value. Examining the figure shows us that the dark correction method was effective since most of the pixels are in the first 4 bins, but not as effective as the interpolation correction method. Again, the first 4 bins represent the error below the noise floor (0.008).
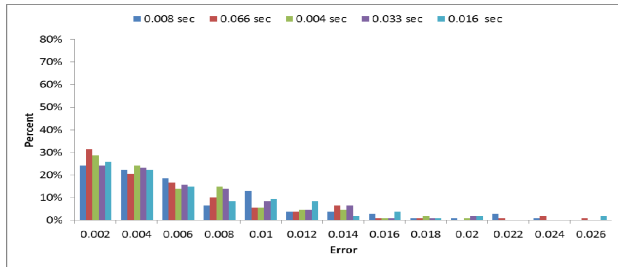


Figure 13: Error distribution of $D_m$

For both methods, there is still a significant number of pixels that have a correction error above the noise floor. This can be seen by creating a distribution on the difference between the $D_m$ error and the $A_m^{(4)}$ error as shown in Figure 14.
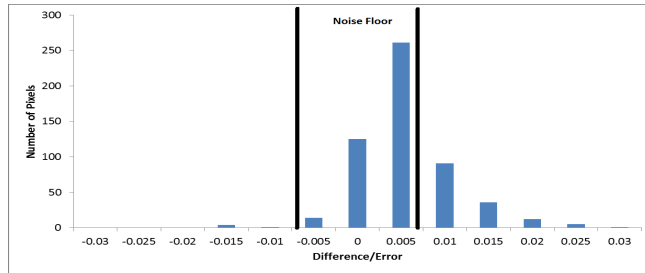


Figure 14: Distribution of $D_m$ error minus $A_m^{(4)}$ error

The pixels that lie on the negative side mean that the dark correction method is more effective for those pixels. The pixels that lie on the positive side mean that the interpolation method is more effective for those pixels. The distribution is centered on 0.005 showing that the interpolation correction method is in general more effective. The majority of the pixels are still within ±0.005 (below the noise floor of ±0.008).

Performing the weighted correction method on the defective pixels to calculate $C_m$, we obtain the error distribution of $C_m$ as shown in Figure 15. Again, this error distribution was obtained by comparing $C_m$ and the true pixel value. When calculating the weighted correction method, we determined the optimized correction weights (α = 0.918, β = 0.548 and ε = 0.005) by minimizing the total absolute error between $C_m$ and the real pixel value using the Excel Solver.

This distribution shows us that the weighted correction method is better since a majority of the pixels have an error below 0.005 and that the number of pixels that have an error above this is statistically insignificant. This is due to the fact that the weighted algorithm gives the advantages of both correction methods.

## VII. CONCLUSIONS

This paper is investigating the effect of hot pixel defects on digital imagers in real images as a preparation for image correction using knowledge of the hot pixel parameters to repair the damage. Our results show that for modest illumination conditions the hot pixel behaves close to the dark field characteristics of the hot pixel. However, at higher illuminations the light interacts with the damage to enhance the hot pixel effect. In our future research we will construct a correction algorithm that will use this illumination knowledge and the surrounding pixel information to get an improved image correction algorithm.
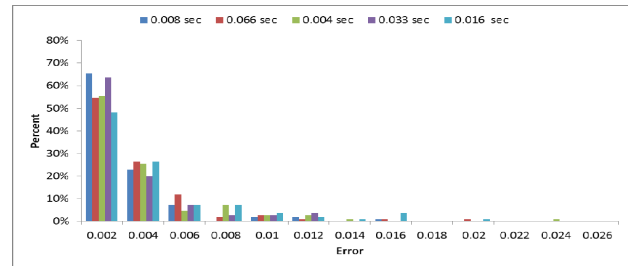


Figure 15: Error distribution of $C_m$

## REFERENCES

[1] J. Dudas, L.M. Wu, C. Jung, G.H. Chapman, Z. Koren, and I. Koren, "Identification of in-field defect development in digital image sensors," *Proc. Electronic Imaging, Digital Photography III*, v6502, 65020Y1-0Y12, San Jose, Jan 2007.

[2] J. Leung, G.H. Chapman, I. Koren, and Z. Koren, "Statistical Identification and Analysis of Defect Development in Digital Imagers," *Proc. SPIE Electronic Imaging, Digital Photography V*, v7250, 742903-1 – 03-12, San Jose, Jan 2009.

[3] J. Leung, G. Chapman, I. Koren, and Z. Koren, "Automatic Detection of In-field Defect Growth in Image Sensors," *Proc. of the 2008 IEEE Intern. Symposium on Defect and Fault Tolerance in VLSI Systems*, 220-228, Boston, MA, Oct. 2008.

[4] J. Leung, G. H. Chapman, I. Koren, Z. Koren, "Tradeoffs in imager design with respect to pixel defect rates," *Proc. of the 2010 Intern. Symposium on Defect and Fault Tolerance in VLSI*, 231-239., Kyoto, Japan, Oct 2010.

[5] J. Leung, J. Dudas, G. H. Chapman, I. Koren, Z. Koren, "Quantitative Analysis of In-Field Defects in Image Sensor Arrays," *Proc. 2007 Intern. Sym on Defect and Fault Tolerance in VLSI*, 526-534, Rome, Italy, Sept 2007.

[6] J. Leung, G.H. Chapman, Y.H. Choi, R. Thomson, I. Koren, and Z. Koren, "Tradeoffs in imager design parameters for sensor reliability," *Proc., Electronic Imaging, Sensors, Cameras, and Systems for Industrial/Scientific Applications XI*, v 7875, 78750I1-0I12, San Jose, Jan. 2011.

[7] A.J.P. Theuwissen, "Influence of terrestrial cosmic rays on the reliability of CCD image sensors. Part 1: experiments at room temperature," *IEEE Transactions on Electron Devices*, Vol. 54 (12), 3260-6, 2007.

[8] A.J.P. Theuwissen, "Influence of terrestrial cosmic rays on the reliability of CCD image sensors. Part 2: experiments at elevated temperature," *IEEE Transactions on Electron Devices*, Vol. 55 (9), 2324-8, 2008.

[9] G.H. Chapman, R. Thomas, I. Koren, and Z. Koren, "Empirical formula for rates of hot pixel defects based on pixel size, sensor area and ISO", *Proc. Electronic Imaging, Sensors, Cameras, and Systems for Industrial/Scientific Applications XIII*, v8659, 86590C-1-C-11 San Francisco, Jan. 2013.

[10] G.H. Chapman, R. Thomas, I. Koren, and Z. Koren, "Correcting high-density hot pixel defects in digital imagers", *Proc. Image Sensors and Imaging Systems 2014,* v9022, 90220G San Francisco, Feb. 2014

[11] Wan, D, Askey, P, Joinson, S, Westlake, A, Butler , R , "Canon EOS 5D Mark II In-depth Review", 2014. Available: http://www. dpreview.com/ reviews/canoneos5dmarkii/ 21